Acta Crystallographica Section B
Structural Science
ISSN 0108-7681

X-ray structure determination of the monoclinic (121 K) and orthorhombic (85 K) phases of langbeinite-type dithallium dicadmium sulfate

A. Guelylah,[a]* G. Madariaga,[a] W. Morgenroth,[b] M. I. Aroyo,[a]† T. Breczewski[c] and E. H. Bocanegra[c]

[a]Departamento de Física de la Materia Condensada, Facultad de Ciencias, Universidad del País Vasco, Apartado 644, Bilbao 48080, Spain, [b]Departamento de Física Aplicada II, Facultad de Ciencias, Universidad del País Vasco, Apartado 644, Bilbao 48080, Spain, and [c]Hamburger Synchrotronstrahlungslabor HASYLAB am Deutschen Electronen-Synchrotron DESY, Notkestrasse 85, D-2000 Hamburg 52, Germany

† On leave of absence from the Faculty of Physics, University of Sofia, Sofia, Bulgaria.

Correspondence e-mail: wmbgugua@lg.ehu.es

Received 24 January 2000
Accepted 3 July 2000

The structures of the monoclinic and the orthorhombic phases of type I langbeinite $Tl_2Cd_2(SO_4)_3$ have been determined at 121 and 85 K, respectively, by X-ray diffraction. A precise analysis of these structures shows the existence of some differences compared to langbeinites of type II. The monoclinic structure differs very little from the high-temperature cubic structure and the distortion relating the monoclinic structure to the cubic one is very small. SO_4 tetrahedra seem to rotate under orthorhombic symmetry in the monoclinic phase. A symmetry distortion analysis of the ferroelectric monoclinic distortion discloses the importance of the secondary modes with orthorhombic symmetry, especially for the O atoms of the SO_4 groups.

1. Introduction

Sulfates with crystal structures of the langbeinite type $A_2B_2(SO_4)_3$, with A = K, NH_4, Tl, Rb, Cs, and B = Mg, Ni, Zn, Fe, Mn, Cd, Co, Ca, have attracted much interest because of their ferroelastic and ferroelectric behaviour and their structural phase transitions.

The common characteristic of langbeinites is their high-temperature cubic structure (space group $P2_13$, $Z = 4$). Many of them undergo phase transitions which are ferroelastic and sometimes also ferroelectric. The sequence of phase transitions allows the classification of langbeinites in two distinct types. Crystals that exhibit a series of phase transitions from cubic ($P2_13$) to orthorhombic ($P2_12_12_1$) across two intermediate, monoclinic ($P2_1$) and triclinic ($P1$), phases belong to type I, for example $Tl_2Cd_2(SO_4)_3$ (TCdS) and $Rb_2Cd_2(SO_4)_3$ (RCdS; Brezina & Glogarova, 1972; Ikeda & Yasuda, 1975; Yamada & Kawano, 1977; Hikita *et al.*, 1978). Crystals of type II undergo a single phase transition from the cubic ($P2_13$) to an orthorhombic ($P2_12_12_1$) phase. To this type belong compounds such as $K_2Cd_2(SO_4)_3$ (KCdS), $K_2Mn_2(SO_4)_3$ (KMnS) and $K_2Ca_2(SO_4)_3$ (KCaS; Abrahams *et al.*, 1978; Hikita *et al.*, 1978; Yamada *et al.*, 1981; Speer & Salje, 1986). Some of the crystals belonging to type I show only one intermediate monoclinic ($P2_1$) phase [$K_2Co_2(SO_4)_3$ (KCoS) and $K_2Zn_2(SO_4)_3$ (KZnS; Yamada *et al.*, 1980)], whereas in others such as $(NH_4)_2Cd_2(SO_4)_3$ [(NH_4)CdS] the monoclinic phase is stable down to liquid helium temperatures (Glogarova & Fousek, 1973; Artman & Boerio-Goates, 1992).

Recent work on langbeinites has been focused on the understanding of the $P2_13 \leftrightarrow P2_12_12_1$ phase transition mechanism. Three different schemes for the transition have been proposed: a displacive mechanism involving rotations of the SO_4 tetrahedra (Lissalde *et al.*, 1979), an order–disorder mechanism (Yamada *et al.*, 1981) and a stereochemical trigger mechanism related to the instabilities around the B^{2+} divalent cation sites (Speer & Salje, 1986; Percival *et al.*, 1989). Nevertheless, the distortion driving the phase transitions in type II langbeinites is more complicated and involves displacements of all the atoms within the unit cell (Hatch *et al.*, 1990; Guelylah, Aroyo & Perez-Mato, 1996). These atomic displacements when analyzed in terms of symmetry modes (Guelylah, Aroyo & Perez-Mato, 1996) show that the phase transition is induced by translations and rotations of the SO_4 groups in combination with Cd and K displacements.

Another model for phase transitions in langbeinites has been proposed by Itoh *et al.* (1992) and Moriyoshi & Itoh (1996). It is based on both the order–disorder and the trigger mechanisms and proposes a nucleation of the low-temperature phase in the cubic one. This model was mainly inspired by the increase of the thermal parameters of O atoms (around the Mn atoms) observed in KMnS in the vicinity of the phase transition temperature (Ukeda *et al.*, 1995). Nevertheless, the temperature region where the thermal amplitudes showed this anomaly has been previously determined to be orthorhombic (Yamada *et al.*, 1981) or an intermediate phase, as in type I langbeinites (Kahrizi & Steinitz, 1988; Kuroiwa *et al.*, 1997).

Previous structure determinations have been carried out on several different langbeinites. The structure of the mineral langbeinite $K_2Mg_2(SO_4)_3$ (KMgS) was first solved by Zemann & Zemann (1957) and was found to be cubic ($P2_13$) at room temperature. Other cubic langbeinites whose structures have been determined are those with K^+ as the monovalent cation, $K_2B_2(SO_4)_3$ [B = Cd (Abrahams *et al.*, 1978), Mn (Yamada *et al.*, 1981), Mg, Ni, Ca, Co and Zn (Speer & Salje, 1986)], (NH_4)CdS (Ng & Calvo, 1975) and TCdS (Cao *et al.*, 1993; Guelylah, Madariaga & Breczewski, 1996). Full structure determinations have been carried out on three orthorhombic K^+ type II langbeinite KCdS (Abrahams *et al.*, 1978), KMnS (Yamada *et al.*, 1981) and KCaS (Speer & Salje, 1986).

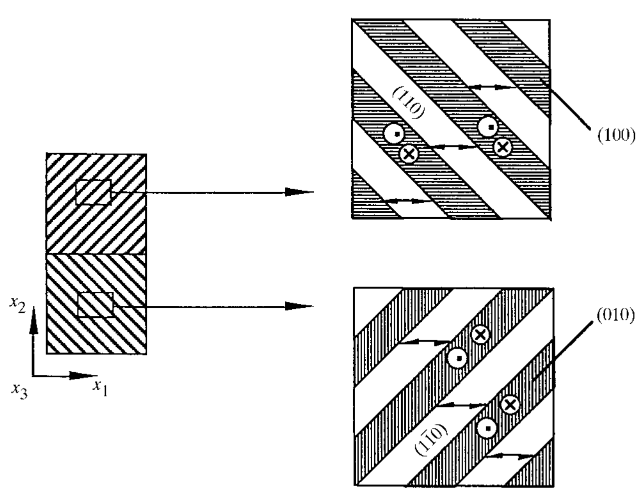

Figure 1
The structure of domains observed in the monoclinic phase (T = 121 K). In the two magnifications the polarization vectors are indicated by arrows. Some permissible domain walls, (100) and (010), which separate the antiparallel $\pm x_3$ domains are drawn. These domain walls are not observed under normal conditions. Only the non-permissible domain walls (110) and $(1\bar{1}0)$ are observed.

However, for type I compounds none of the low-temperature phases have been determined, probably because of the difficult domain structures appearing in the monoclinic (six orientational states) and triclinic (12 orientational states) phases.

The main goal of the present work is to study the mechanism of the structural phase transitions in type I langbeinite. Up to now, the mechanisms responsible for the phase transition in type I langbeinite and the factors behind the different phase transition schemes in langbeinite compounds were still obscure owing to the lack of structural information corresponding to the low-temperature phases of type I compounds. In particular, the low-temperature monoclinic and orthorhombic structures of TCdS have been solved and precisely analysed to find out the factors involved in the phase transitions of type I langbeinites.

2. Experimental

2.1. Preliminaries

Single crystals of TCdS were grown using the technique described previously (Guelylah, Aroyo & Perez-Mato, 1996). The crystal habit is similar to that obtained by Brezina & Havránková (1974) and the tetrahedral pyramid shape surrounded by {111} faces and accompanied with {100} facets along the edges of the pyramid. DSC (differential scanning calorimetry) measurements in the temperature range 100–300 K show two phase transitions at 127.7 K (I $\leftrightarrow$ II)[1] and 118.5 K (II $\leftrightarrow$ III), in good agreement with previous works (Cao *et al.*, 1993; Brezina & Glogarova, 1972; Franke *et al.*, 1975). The last phase transition (III $\leftrightarrow$ IV) at 92 K (Cao *et al.*, 1993; Brezina & Glogarova, 1972; Franke *et al.*, 1975) is below the minimum temperature accessible by the DSC instrument.

A (001) plate of *ca* 3 × 3 × 0.3 mm^3 was polished and prepared for optical observation of domain structures under a polarizing microscope. Below 128 K, the observed domain pattern consists of stripes with (110) and $(1\bar{1}0)$ boundaries located symmetrically with respect to the [100] direction (Fig. 1). One stripe is a set of 'x_1 or x_2 domains'[2] and is sandwiched by two dense networks of antiparallel '$\pm x_3$ domains', divided by (010) or (100) domain walls. The same domain patterns were observed in the monoclinic phase of (NH_4)CdS (Glogarova *et al.*, 1972; Glogarova & Fousek, 1973) and TCdS (Brezina & Glogarova, 1972).

In the triclinic phase (III) below 118.5 K, a very complicated domain structure appears in the same configuration as described by Brezina & Glogarova (1972). In the low-temperature orthorhombic phase (IV) and near the phase transition temperature, the observed domain structure is characterized by sharp boundaries along the [110] or $[1\bar{1}0]$ directions. After one cycle of heating and cooling, the sample presents two zones with a different domain structure sepa-

[1] I, II, III and IV represent the cubic, monoclinic, triclinic and orthorhombic phases, respectively.
[2] In x_1, x_2 and x_3 domains, the spontaneous polarization, P_s, is parallel to the axes x_1, x_2 and x_3, respectively.

rated by a (100) domain boundary. One of them is single domain, the other is constituted by a dense network of parallel domains along the [110] direction. Heating up to room temperature, all the phase transitions are reversible.

Using a spherical sample of radius 0.2 mm, precession photographs were taken at appropriate temperatures in the four phases. Below the I $\leftrightarrow$ II phase transition temperature the lattice distortion was so small that no deviation from the cubic symmetry could be detected. A very long exposure time was necessary to observe some very weak additional reflections violating the $P2_13$ systematic absences along the crystallographic axes. In the triclinic phase, the precession photographs were identical to those obtained in the monoclinic phase. The lattice distortion with respect to the cubic and monoclinic phases was again inappreciable. No superlattice reflections as predicted by Dvorák (1972) were observed in the monoclinic and triclinic phases, even for exposures of ~100 h. In phase IV, the systematic absences and the symmetry of the diagrams were in good agreement with the $P2_12_12_1$ space group. The monoclinic ($P2_1$) symmetry of phase II was then confirmed by the X-ray precession photograph in combination with optical observation of the domains.

2.2. Data collection

At 85 K, diffracted intensities were measured with graphite-monochromated Mo $K\alpha$ radiation (λ = 0.7107 Å) on a CAD-4 diffractometer equipped with an Oxford Cryosystem open gas-flow cryostat (Cosier & Glazer, 1986). The temperature stability was within $\pm$0.3 K during the time of the measurement. Details of data collection are summarized in Table 1.[3] The orientation matrix of the crystal was refined at room temperature from 25 reflections, then the temperature was lowered down to 130 K with a cooling rate of 2° min^{-1} and then to 85 K with a rate of 1° min^{-1}. Once in the orthorhombic (IV) phase the orientation matrix was refined with the previous 25 reflections [a = 10.327 (3), b = 10.345 (4) and c = 10.406 (5) Å]. In the monoclinic (II) and the triclinic (III) phases the orientation matrices were also refined confirming the very small deviation from the cubic symmetry, as observed by precession photographs. The stability of the measurement was checked periodically using three standard reflections. The overall decay was ~4% and linear; Lp, absorption corrections and data reduction were carried out using the program *JANA*98 (Petricek & Ducek, 1998).

At 121 K, data collection was carried out using synchrotron radiation on a Huber four-circle Kappa diffractometer at HASYLAB-DESY (Hamburg, Germany) beamline F1. The wavelength was set to 0.5502 Å *via* an Si(111) double crystal monochromator. For strong reflections the intensity was reduced by the insertion of the appropriate filter combinations. In order to reduce the influence of air scattering, a copper tube of ~20 cm in length was located at the entrance of the detector. The temperature of the measurement was reached and controlled using a cryostat similar to the previous one (Cosier & Glazer, 1986). The temperature stability was within $\pm$0.2K during the time of the measurement.

The orientation matrix of the crystal was first refined at room temperature from the optimized angular setting of 8 reflections ($|h|$, $|k|$, $|l|$ = 8, 8, 8; 2θ = 43.033°); a = 10.39 (4), b = 10.39 (4), c = 10.39 (4) Å. Then the temperature of the crystal was lowered down to 130 K with a cooling rate of 2° min^{-1} and then to 121 K with a rate of 1° min^{-1}. Once in the monoclinic phase, the orientation matrix was refined using the previous 8 reflections [a = 10.36 (4), b = 10.35 (4), c = 10.35 (4) Å, α = 89.9 (3), β = 90.0 (3) and γ = 90.0 (3)°]. Some systematic absences of the $P2_13$ space group (0k0: $k = 2n + 1$) were scanned in the vicinity of the I $\leftrightarrow$ II phase transition temperature. Fig. 2 show the profile of the reflections (0,−5,0) and (0,15,0) at 121 K. For the (0, 15, 0) profile the contribution of more than one orientation state can be seen. Nevertheless, reflections corresponding to lower 2θ angles [case of (0,5,0)] are less separated due to the small lattice distortion.

Two standard reflections (4,0,0) and (0,4,0) were used as check reflections and remeasured every 20 min and at the beginning of each synchrotron fill.

Intensities were corrected for intensity decay of synchrotron radiation using the program *AVSORT* (Eichhorn, 1992). Integration of the intensities using the Lehmann–Larsen

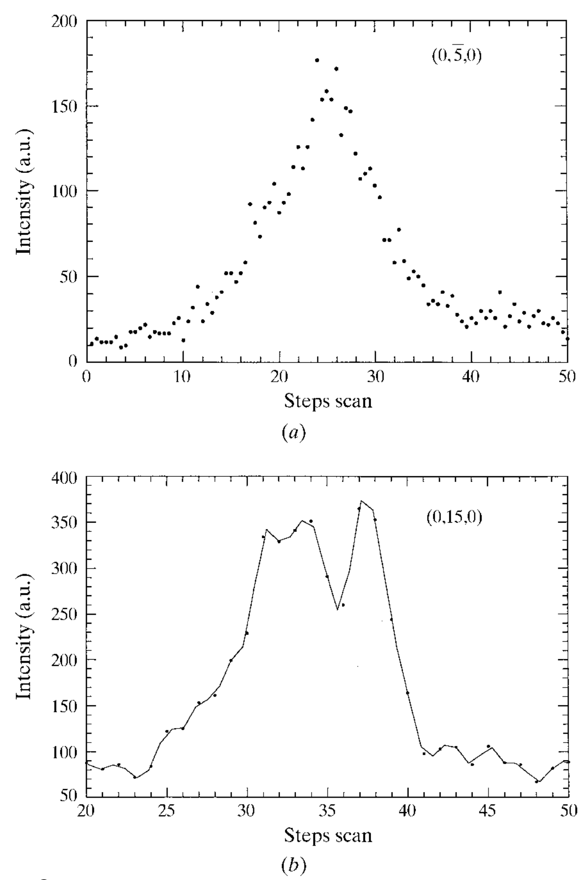

Figure 2
Profiles of the (0, $\bar{5}$, 0) and (0, 15, 0) reflections. In the (0, 15, 0) case, the contribution of more than one domain is observed.

[3] Supplementary data for this paper are available from the IUCr electronic archives (Reference: NA0103). Services for accessing these data are described at the back of the journal.

Table 1
Experimental details.

	121 K	85 K
Crystal data		
Chemical formula	$Tl_2Cd_2(SO_4)_3$	$Tl_2Cd_2(SO_4)_3$
Chemical formula weight	921.7	921.7
Cell setting	Monoclinic	Orthorhombic
Space group	$P2_1$	$P2_12_12_1$
a (Å)	10.356 (4)	10.327 (3)
b (Å)	10.350 (2)	10.345 (4)
c (Å)	10.353 (6)	10.406 (5)
γ (°)	90.04 (3)	90
V (Å^3)	1109.7 (8)	1111.7 (8)
Z	4	4
D_x (Mg m^{-3})	5.515	5.505
Radiation type	Synchrotron	Mo $K\alpha$
Wavelength (Å)	0.5502	0.71073
No. of reflections for cell parameters	27	25
θ range (°)	7.41–29.22	5.1–28.7
μ (mm^{-1})	17.53	33.298
Temperature (K)	121	85
Crystal form	Parallelepiped	Sphere
Crystal size (mm)	0.59 × 0.35 × 0.35	0.12 (radius)
Crystal colour	Colourless	Colourless
Data collection		
Diffractometer	Huber CAD-4 κ geometry	Enraf–Nonius CAD-4
Data collection method	$\theta/2\theta$ scans	$\theta/2\theta$ scans
Absorption correction	Analytical	Spherical
T_{min}	0.009	0.002
T_{max}	0.046	0.015
No. of measured reflections	9312	5303
No. of independent reflections	8392	4985
No. of observed reflections	8392	4028
Criterion for observed reflections	$I > 3\sigma(I)$	$I > 3\sigma(I)$
θ_{max} (°)	20.02	34.96
Range of h, k, l	$-12 \rightarrow h \rightarrow 12$	$0 \rightarrow h \rightarrow 16$
	$-12 \rightarrow k \rightarrow 12$	$0 \rightarrow k \rightarrow 16$
	$-12 \rightarrow l \rightarrow 12$	$-16 \rightarrow l \rightarrow 16$
No. of standard reflections	2	3
Frequency of standard reflections	Every 20 min	Every 120 min
Intensity decay (%)	0	4
Refinement		
Refinement on	F	F
R	0.044	0.057
wR	0.064	0.060
S	13.78	2.33
No. of reflections used in refinement	8392	4985
No. of parameters used	132	67
Weighting scheme	$w = 1/\sigma^2(F)$	$w = 1/\sigma^2(F)$
$(\Delta/\sigma)_{max}$	0.0007	0.0004
$\Delta\rho_{max}$ (e Å^{-3})	2.43	4.77
$\Delta\rho_{min}$ (e Å^{-3})	−1.86	−4.73
Extinction method	*B–C* type 1 Gaussian isotropic	*B–C* type 1 Gaussian isotropic
Extinction coefficient	0.182 (4)	0.015 (3)
Source of atomic scattering factors	*International Tables for Crystallography* (1992, Vol. C)	*International Tables for Crystallography* (1992, Vol. C)
Domain fractions		
f_1	34.2 (2)	79.1 (2)
f_2	2.4 (2)	10.5 (2)
f_3	30.6 (2)	10.4 (2)
f_4	0.0 (2)	–
f_5	28.8 (2)	–
f_6	4.0 (2)	–
Computer programs		
Data collection	*DIF*4 (Eichhorn & Morgenroth, 1996)	*CAD*-4*VPC* (Enraf–Nonius, 1989)
Cell refinement	*DIF*4 (Eichhorn & Morgenroth, 1996)	*CAD*-4*VPC* (Enraf–Nonius, 1989)
Data reduction	*AVSORT*, *REDUCE*, *XtalABSORB* (Eichhorn, 1987, 1992)	*JANA*98 (Hall *et al.*, 1992)
Structure solution	*JANA*98 (Petricek & Dusek, 1998)	*JANA*98 (Petricek & Dusek, 1998)
Structure refinement	*JANA*98 (Petricek & Dusek, 1998)	*JANA*98 (Petricek & Dusek, 1998)
Preparation of material for publication	*JANA*98 (Petricek & Dusek, 1998)	*JANA*98 (Petricek & Dusek, 1998)

Table 2
Relevant transformations and relations for superposition of indices from pertinent domains.

$$\begin{bmatrix} h \\ k \\ l \end{bmatrix}^1 = \begin{bmatrix} 1 & 0 & 0 \\ 0 & 1 & 0 \\ 0 & 0 & 1 \end{bmatrix} \begin{bmatrix} h \\ k \\ l \end{bmatrix}^1 \qquad \begin{bmatrix} h \\ k \\ l \end{bmatrix}^4 = \begin{bmatrix} -1 & 0 & 0 \\ 0 & 1 & 0 \\ 0 & 0 & -1 \end{bmatrix} \begin{bmatrix} h \\ k \\ l \end{bmatrix}^1$$

$$\begin{bmatrix} h \\ k \\ l \end{bmatrix}^2 = \begin{bmatrix} 0 & 1 & 0 \\ 0 & 0 & 1 \\ 1 & 0 & 0 \end{bmatrix} \begin{bmatrix} h \\ k \\ l \end{bmatrix}^1 \qquad \begin{bmatrix} h \\ k \\ l \end{bmatrix}^5 = \begin{bmatrix} 0 & 1 & 0 \\ 0 & 0 & -1 \\ -1 & 0 & 0 \end{bmatrix} \begin{bmatrix} h \\ k \\ l \end{bmatrix}^1$$

$$\begin{bmatrix} h \\ k \\ l \end{bmatrix}^3 = \begin{bmatrix} 0 & 0 & 1 \\ 1 & 0 & 0 \\ 0 & 1 & 0 \end{bmatrix} \begin{bmatrix} h \\ k \\ l \end{bmatrix}^1 \qquad \begin{bmatrix} h \\ k \\ l \end{bmatrix}^6 = \begin{bmatrix} 0 & 0 & -1 \\ 1 & 0 & 0 \\ 0 & -1 & 0 \end{bmatrix} \begin{bmatrix} h \\ k \\ l \end{bmatrix}^1$$

algorithm (Lehman & Larsen, 1974) and *Lp* corrections were carried out using the program *REDUCE* (Eichhorn, 1987).

An analytical absorption correction based on the shape of the specimen was applied, using the program *Xtal*3.2 (Hall *et al.*, 1992). Owing to the presence of several twin domain in the sample, symmetry-equivalent reflections were not averaged.

Owing to the presence of domains in the monoclinic phase (6), the lattice parameters determined from the multiply twinned single-crystal reflections of the low-temperature phase are biased by this systematic error. More accurate unit-cell parameters at 121 K were obtained from powder diffraction measurements. They were performed on a Stoe focusing monochromatic beam transmission diffractometer equipped with a linear position detector. The powdered sample was inserted in a Lindemann capillary of diameter 0.3 mm. The measured region was 10–89.94° (2θ), λ(Cu $K\alpha_1$) = 1.54056 Å. The lattice parameters obtained after least-squares refinement were a = 10.356 (4), b = 10.350 (2), c = 10.353 (6) Å and γ = 90.04 (3)°. They perfectly coincide, within experimental error, with those obtained during the single-crystal data collection.

2.3. Data analysis and structure refinement

Starting structural models for the (monoclinic and orthorhombic) low-temperature phases were extrapolated from the room-temperature cubic structure (Guelylah, Madariaga & Breczewski, 1996). In the monoclinic phase the refinement was carried out in the space group $P112_1$. In the orthorhombic phase the space group is $P2_12_12_1$. The twin operations which relate the different superimposed reflections in the low-symmetry phases are those symmetry operations of the cubic phase lost in the phase transition. Table 2 shows the six matrices that relate reflections originating from the six orientation states present in the monoclinic phase. The first three matrices are related by a threefold axis and also represent the relation between the three orientation states in the orthorhombic phase. The three remaining matrices (4, 5 and 6) represent the antiparallel orientation states (the 'ferroelectric domains') of the first ones in the monoclinic phase. Initial values of the domain fractions were equal for all the orientation states, 1/6 and 1/3 in the monoclinic and orthorhombic phases, respectively. In both phases, the scattering factors for neutral atoms Tl, Cd, S and O were taken from the *International Tables for Crystallography* (1992, Vol. C).

Table 3
Fractional atomic coordinates and equivalent isotropic displacement parameters (Å^2) for 121 K.

$$U_{\rm eq} = (1/3)\Sigma_i\Sigma_j U^{ij}a^ia^j\mathbf{a}_i.\mathbf{a}_j.$$

	x	y	z	$U_{\rm eq}$
121 K				
Tl21	0.80235 (4)	0.05287 (4)	0.043756	0.0136 (1)
Tl11	0.56739 (4)	0.81699 (5)	0.81002 (6)	0.0144 (1)
Tl12	0.06866 (4)	0.68261 (4)	0.17413 (6)	0.0149 (1)
Tl22	0.30273 (4)	0.44800 (4)	0.93967 (7)	0.0145 (1)
Cd11	0.08851 (6)	0.33194 (9)	0.32064 (9)	0.00722 (8)
Cd12	0.58546 (7)	0.16893 (9)	0.66497 (8)	0.00957 (8)
Cd21	0.33856 (7)	0.59002 (7)	0.57932 (9)	0.00526 (7)
Cd22	0.83717 (7)	0.91000 (7)	0.40177 (9)	0.00797 (8)
S1*a*	0.0298 (2)	0.6217 (2)	0.5043 (2)	0.0046 (1)
O1*a*	−0.0582 (3)	0.7173 (3)	0.4514 (4)	0.0130 (4)
O2*a*	0.1604 (2)	0.6676 (4)	0.4767 (4)	0.0054 (4)
O3*a*	0.0059 (4)	0.4974 (3)	0.4361 (4)	0.0118 (5)
O4*a*	0.0049 (4)	0.5999 (4)	0.6455 (3)	0.0154 (5)
S1*b*	0.5331 (2)	0.8839 (2)	0.4799 (2)	0.0046 (1)
O1*b*	0.4452 (3)	0.7855 (3)	0.5279 (4)	0.0130 (4)
O2*b*	0.6637 (2)	0.8377 (4)	0.5066 (4)	0.0054 (4)
O3*b*	0.5080 (4)	1.0049 (3)	0.5533 (4)	0.0118 (5)
O4*b*	0.5091 (4)	0.9117 (4)	0.3397 (3)	0.0154 (5)
S1*c*	0.2647 (2)	0.2710 (2)	0.6201 (2)	0.0046 (1)
O1*c*	0.2257 (4)	0.1843 (4)	0.7233 (3)	0.0130 (4)
O2*c*	0.2252 (4)	0.4008 (3)	0.6593 (4)	0.0054 (4)
O3*c*	0.1942 (4)	0.2321 (4)	0.5011 (3)	0.0118 (5)
O4*c*	0.4065 (2)	0.2596 (4)	0.5928 (4)	0.0154 (5)
S1*d*	0.7626 (2)	0.2300 (2)	0.3648 (2)	0.0046 (1)
O1*d*	0.7322 (4)	0.3210 (4)	0.2625 (3)	0.0130 (4)
O2*d*	0.7187 (4)	0.1033 (3)	0.3205 (4)	0.0054 (4)
O3*d*	0.6891 (4)	0.2692 (4)	0.4818 (3)	0.0118 (5)
O4*d*	0.9036 (2)	0.2339 (4)	0.3982 (4)	0.0154 (5)
S1*e*	0.3767 (2)	0.5145 (2)	0.2718 (2)	0.0046 (1)
O1*e*	0.4782 (3)	0.4691 (4)	0.1864 (4)	0.0130 (4)
O2*e*	0.4319 (4)	0.5181 (4)	0.4018 (3)	0.0054 (4)
O3*e*	0.2692 (3)	0.4192 (4)	0.2669 (4)	0.0118 (5)
O4*e*	0.3244 (4)	0.6423 (2)	0.2277 (4)	0.0154 (5)
S1*f*	0.8772 (2)	0.9859 (2)	0.7125 (2)	0.0046 (1)
O1*f*	0.9815 (3)	1.0335 (4)	0.7933 (4)	0.0130 (4)
O2*f*	0.9290 (4)	0.9755 (4)	0.5816 (3)	0.0054 (4)
O3*f*	0.7713 (3)	1.0830 (4)	0.7157 (4)	0.0118 (5)
O4*f*	0.8239 (4)	0.8610 (2)	0.7636 (4)	0.0154 (5)
85 K				
Tl1	0.81231 (7)	0.82841 (7)	0.81649 (7)	0.0076 (1)
Tl2	0.05831 (7)	0.04009 (7)	0.05051 (7)	0.0093 (2)
Cd1	0.3325 (1)	0.3163 (1)	0.3408 (1)	0.0050 (3)
Cd2	0.5790 (1)	0.5998 (1)	0.5943 (1)	0.0052 (3)
S1*ab*	0.2602 (4)	0.6201 (4)	0.5082 (3)	0.0045
O1*ab*	0.175 (1)	0.700 (1)	0.434 (1)	0.0118
O2*ab*	0.3937 (8)	0.673 (1)	0.496 (1)	0.0095
O3*ab*	0.253 (1)	0.4866 (8)	0.454 (1)	0.0094
O4*ab*	0.221 (1)	0.616 (1)	0.6443 (8)	0.0071
S1*cd*	0.5234 (3)	0.2850 (3)	0.6269 (4)	0.0045
O1*cd*	0.511 (1)	0.195 (1)	0.731 (1)	0.0118
O2*cd*	0.491 (1)	0.4162 (8)	0.676 (1)	0.0095
O3*cd*	0.429 (1)	0.245 (1)	0.5252 (9)	0.0094
O4*cd*	0.6553 (8)	0.284 (1)	0.573 (1)	0.0071
S1*ef*	0.6325 (4)	0.5072 (3)	0.2860 (3)	0.0045
O1*ef*	0.736 (1)	0.440 (1)	0.222 (1)	0.0118
O2*ef*	0.682 (1)	0.554 (1)	0.4122 (8)	0.0095
O3*ef*	0.5245 (9)	0.413 (1)	0.305 (1)	0.0094
O4*ef*	0.585 (1)	0.6170 (8)	0.209 (1)	0.0071

Initial steps of the refinement were made with isotropic thermal displacement parameters. First results led to unrealistic atomic positions, especially for O atoms, as is normally expected for twinned crystals. Therefore, given the quasi-rigid behaviour of the SO_4 groups during the phase transition in langbeinite (Abrahams *et al.*, 1978; Yamada *et al.*, 1981), the position of the atoms forming the tetrahedral groups were refined using the so-called model molecules (Petricek & Dusek, 1998). The positions of model molecules are defined by three rotation angles and a position vector that can be refined. The atoms in a model molecule have their own atomic parameters which can be refined. The only restriction is that all the model molecules are identical in shape. Then the model molecule is not considered strictly rigid because its geometry can change during the refinement. The temperature parameters of specific molecules can also be refined as molecular parameters, together with its rotational and translational parameters. After several refinement cycles with anisotropic thermal parameters, the R values obtained were ~16 and 12% for the monoclinic and orthorhombic phases, respectively. Moreover, the monoclinic structure showed no significant changes with respect to that of the cubic phase.

These results led us to analyse the possible factors that can affect the final result, for instance, unsuitable structural models or screening among the different domains due to the high absorption of the material. To check the goodness of the initial atomic positions, a Patterson map was calculated from the diffracted monoclinic intensities. The map revealed the position of the heaviest atoms, Tl and Cd. These positions coincide exactly with that of the model extrapolated from the cubic structure. Secondly, we correct the intensities for absorption empirically (Flack, 1974). Nevertheless, the results obtained were even worse than the previous ones. Therefore, after these tests we concluded that the origin of the problem is probably the high absorption of the material combined with the domain structure. The screening caused by the different domains provokes an incorrect absorption correction. During the refinement, we observed that approximately half of the total observed intensities (I_o) are very well adjusted to the calculated ones (I_c). The remaining reflections can be classified in different groups according to the differences ($I_o - I_c$). Within each group the agreement between I_o and I_c is almost exact if an appropriate multiplicative factor is applied to I_o (or I_c). So the problem seems to be related to the scale factor. The whole data set could be rescaled using a combination of two options of the program *REFINE*/*JANA*98 (Petricek & Dusek, 1998). The first option detects the observed intensities which deviate significantly from the calculated ones. The second option isolates the intensities selected by the previous one, thus removing them from

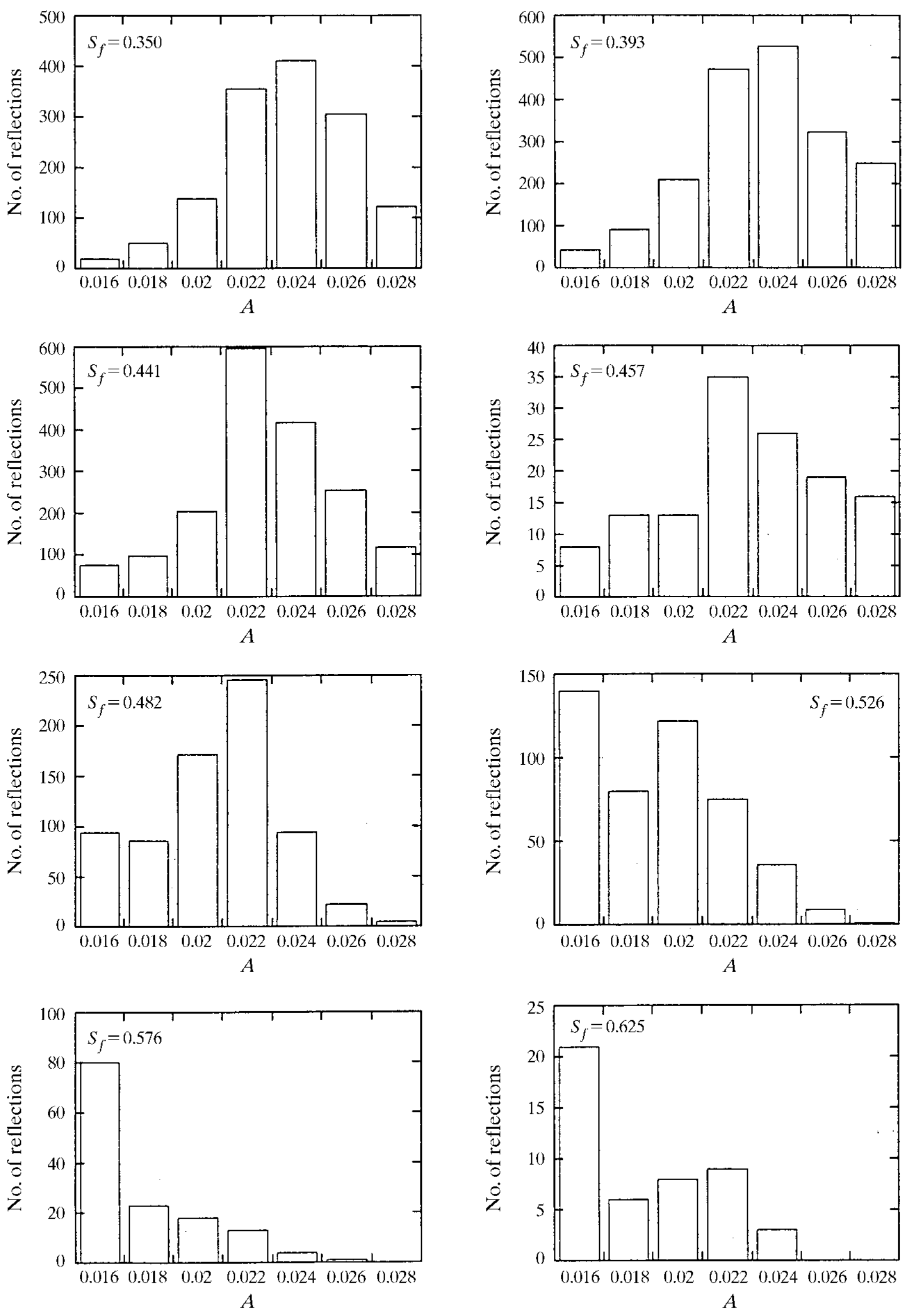

Figure 3
Groups of structure factors used for refinement of the monoclinic structure at 121 K. Each histogram represents a group of structure factors, corresponding to the same scale factor V_s the transmission factor A.

Table 4
Selected geometric parameters (Å, °).

121 K			
Tl21—O2*a*$^{\mathrm{i}}$	3.000 (4)	Cd12—O3*b*$^{\mathrm{xii}}$	2.205 (4)
Tl21—O1*b*$^{\mathrm{i}}$	3.066 (4)	Cd12—O4*b*$^{\mathrm{vi}}$	2.220 (4)
Tl21—O3*b*$^{\mathrm{i}}$	3.270 (4)	Cd12—O4*c*	2.208 (3)
Tl21—O1*c*$^{\mathrm{ii}}$	3.092 (4)	Cd12—O3*d*	2.413 (4)
Tl21—O3*c*$^{\mathrm{ii}}$	2.983 (4)	Cd12—O4*e*$^{\mathrm{vi}}$	2.260 (3)
Tl21—O2*d*	3.039 (4)	Cd12—O3*f*$^{\mathrm{xii}}$	2.185 (4)
Tl21—O1*f*$^{\mathrm{iii}}$	3.195 (4)	Cd21—O2*a*	2.276 (3)
Tl21—O2*f*$^{\mathrm{iv}}$	2.825 (4)	Cd21—O1*b*	2.365 (4)
Tl11—O1*b*	3.200 (4)	Cd21—O2*c*	2.429 (3)
Tl11—O3*b*$^{\mathrm{v}}$	3.218 (4)	Cd21—O1*d*$^{\mathrm{vi}}$	2.232 (4)
Tl11—O4*b*$^{\mathrm{v}}$	2.934 (4)	Cd21—O1*e*$^{\mathrm{vi}}$	2.281 (4)
Tl11—O3*c*$^{\mathrm{vi}}$	3.205 (4)	Cd21—O2*e*	2.207 (3)
Tl11—O4*c*$^{\mathrm{vi}}$	3.045 (5)	Cd22—O1*a*$^{\mathrm{xiii}}$	2.328 (4)
Tl11—O2*d*$^{\mathrm{vi}}$	3.078 (4)	Cd22—O2*b*	2.228 (3)
Tl11—O1*e*$^{\mathrm{vi}}$	3.259 (4)	Cd22—O1*c*$^{\mathrm{i}}$	2.188 (4)
Tl11—O3*e*$^{\mathrm{vi}}$	3.008 (4)	Cd22—O2*d*$^{\mathrm{xiv}}$	2.494 (3)
Tl11—O4*f*	2.737 (4)	Cd22—O1*f*$^{\mathrm{xv}}$	2.265 (4)
Tl12—O1*a*	3.177 (4)	Cd22—O2*f*	2.197 (3)
Tl12—O2*a*	3.277 (4)	S1*a*—O1*a*	1.452 (4)
Tl12—O3*a*$^{\mathrm{vii}}$	3.184 (4)	S1*a*—O2*a*	1.462 (3)
Tl12—O4*a*$^{\mathrm{vii}}$	3.035 (4)	S1*a*—O3*a*	1.488 (4)
Tl12—O2*c*$^{\mathrm{vii}}$	3.166 (4)	S1*a*—O4*a*	1.501 (4)
Tl12—O3*d*$^{\mathrm{i}}$	3.241 (4)	S1*b*—O1*b*	1.452 (4)
Tl12—O4*d*$^{\mathrm{i}}$	2.998 (5)	S1*b*—O2*b*	1.462 (3)
Tl12—O4*e*	2.738 (4)	S1*b*—O3*b*	1.488 (4)
Tl12—O1*f*$^{\mathrm{viii}}$	3.229 (4)	S1*b*—O4*b*	1.501 (4)
Tl12—O3*f*$^{\mathrm{viii}}$	2.969 (4)	S1*c*—O1*c*	1.452 (4)
Tl22—O1*a*$^{\mathrm{ix}}$	3.058 (4)	S1*c*—O2*c*	1.462 (4)
Tl22—O3*a*$^{\mathrm{ix}}$	3.247 (4)	S1*c*—O3*c*	1.488 (4)
Tl22—O2*b*$^{\mathrm{vi}}$	3.057 (4)	S1*c*—O4*c*	1.501 (3)
Tl22—O2*c*	3.051 (4)	S1*d*—O1*d*	1.452 (4)
Tl22—O1*d*$^{\mathrm{vi}}$	3.036 (4)	S1*d*—O2*d*	1.462 (4)
Tl22—O3*d*$^{\mathrm{vi}}$	2.960 (4)	S1*d*—O3*d*	1.488 (4)
Tl22—O1*e*$^{\mathrm{x}}$	3.142 (4)	S1*d*—O4*d*	1.501 (3)
Tl22—O2*e*$^{\mathrm{vi}}$	2.798 (4)	S1*e*—O1*e*	1.452 (4)
Cd11—O3*a*	2.258 (4)	S1*e*—O2*e*	1.462 (4)
Cd11—O4*a*$^{\mathrm{vii}}$	2.173 (4)	S1*e*—O3*e*	1.488 (4)
Cd11—O3*c*	2.399 (4)	S1*e*—O4*e*	1.501 (4)
Cd11—O4*d*$^{\mathrm{xi}}$	2.311 (3)	S1*f*—O1*f*	1.452 (4)
Cd11—O3*e*	2.150 (4)	S1*f*—O2*f*	1.462 (4)
Cd11—O4*f*$^{\mathrm{i}}$	2.272 (3)	S1*f*—O3*f*	1.488 (4)
		S1*f*—O4*f*	1.501 (4)
O1*a*—S1*a*—O2*a*	106.6 (3)	O1*d*—S1*d*—O2*d*	106.6 (3)
O1*a*—S1*a*—O3*a*	107.8 (3)	O1*d*—S1*d*—O3*d*	107.8 (3)
O1*a*—S1*a*—O4*a*	111.2 (3)	O1*d*—S1*d*—O4*d*	111.2 (3)
O2*a*—S1*a*—O3*a*	109.9 (3)	O2*d*—S1*d*—O3*d*	109.9 (3)
O2*a*—S1*a*—O4*a*	113.5 (3)	O2*d*—S1*d*—O4*d*	113.5 (3)
O3*a*—S1*a*—O4*a*	107.6 (3)	O3*d*—S1*d*—O4*d*	107.6 (3)
O1*b*—S1*b*—O2*b*	106.6 (3)	O1*e*—S1*e*—O2*e*	106.6 (2)
O1*b*—S1*b*—O3*b*	107.8 (3)	O1*e*—S1*e*—O3*e*	107.8 (3)
O1*b*—S1*b*—O4*b*	111.2 (3)	O1*e*—S1*e*—O4*e*	111.2 (3)
O2*b*—S1*b*—O3*b*	109.9 (3)	O2*e*—S1*e*—O3*e*	109.9 (3)
O2*b*—S1*b*—O4*b*	113.5 (3)	O2*e*—S1*e*—O4*e*	113.5 (3)
O3*b*—S1*b*—O4*b*	107.6 (3)	O3*e*—S1*e*—O4*e*	107.6 (3)
O1*c*—S1*c*—O2*c*	106.6 (3)	O1*f*—S1*f*—O2*f*	106.6 (2)
O1*c*—S1*c*—O3*c*	107.8 (3)	O1*f*—S1*f*—O3*f*	107.8 (2)
O1*c*—S1*c*—O4*c*	111.2 (3)	O1*f*—S1*f*—O4*f*	111.2 (3)
O2*c*—S1*c*—O3*c*	109.9 (3)	O2*f*—S1*f*—O3*f*	109.9 (3)
O2*c*—S1*c*—O4*c*	113.5 (3)	O2*f*—S1*f*—O4*f*	113.5 (3)
O3*c*—S1*c*—O4*c*	107.6 (3)	O3*f*—S1*f*—O4*f*	107.6 (2)

Symmetry codes: (i) $1-x, 1-y, z-\frac{1}{2}$; (ii) $1-x, -y, z-\frac{1}{2}$; (iii) $x, y-1, z-1$; (iv) $2-x, 1-y, z-\frac{1}{2}$; (v) $1-x, 2-y, \frac{1}{2}+z$; (vi) $1-x, 1-y, \frac{1}{2}+z$; (vii) $-x, 1-y, z-\frac{1}{2}$; (viii) $1-x, 2-y, z-\frac{1}{2}$; (ix) $-x, 1-y, \frac{1}{2}+z$; (x) $x, y, 1+z$; (xi) $x-1, y, z$; (xii) $x, y-1, z$; (xiii) $1+x, y, z$; (xiv) $x, 1+y, z$; (xv) $2-x, 2-y, z-\frac{1}{2}$.

85 K			
Tl1—O1*ab*$^{\mathrm{i}}$	2.98 (1)	Cd1—O4*ef*$^{\mathrm{vi}}$	2.289 (9)
Tl1—O3*ab*$^{\mathrm{ii}}$	2.98 (1)	Cd1—O3*cd*	2.29 (1)
Tl1—O4*ab*$^{\mathrm{ii}}$	3.03 (1)	Cd1—O4*cd*$^{\mathrm{ix}}$	2.287 (9)
Tl1—O1*ef*$^{\mathrm{iii}}$	2.99 (1)	Cd2—O1*ab*$^{\mathrm{i}}$	2.31 (1)

Table 4 (continued)

Tl1—O3*ef*$^{\mathrm{iii}}$	3.01 (1)	Cd2—O2*ab*	2.296 (9)
Tl1—O4*ef*$^{\mathrm{i}}$	2.89 (1)	Cd2—O1*ef*$^{\mathrm{iii}}$	2.36 (1)
Tl1—O2*cd*$^{\mathrm{ii}}$	3.27 (1)	Cd2—O2*ef*	2.224 (9)
Tl1—O3*cd*$^{\mathrm{ii}}$	3.11 (1)	Cd2—O1*cd*$^{\mathrm{ii}}$	2.27 (1)
Tl1—O4*cd*$^{\mathrm{iii}}$	2.92 (1)	Cd2—O2*cd*	2.269 (9)
Tl2—O1*ab*$^{\mathrm{iv}}$	2.93 (1)	S1*ab*—O1*ab*	1.44 (1)
Tl2—O2*ab*$^{\mathrm{v}}$	3.06 (1)	S1*ab*—O2*ab*	1.487 (9)
Tl2—O3*ab*$^{\mathrm{iv}}$	3.27 (1)	S1*ab*—O3*ab*	1.50 (1)
Tl2—O2*ef*$^{\mathrm{vi}}$	2.72 (1)	S1*ab*—O4*ab*	1.475 (9)
Tl2—O4*ef*$^{\mathrm{vii}}$	3.16 (1)	S1*ef*—O1*ef*	1.44 (1)
Tl2—O1*cd*$^{\mathrm{viii}}$	3.16 (1)	S1*ef*—O2*ef*	1.49 (1)
Tl2—O2*cd*$^{\mathrm{ix}}$	2.96 (1)	S1*ef*—O3*ef*	1.50 (1)
Tl2—O3*cd*$^{\mathrm{viii}}$	2.96 (1)	S1*ef*—O4*ef*	1.47 (1)
Cd1—O3*ab*	2.27 (1)	S1*cd*—O1*cd*	1.44 (1)
Cd1—O4*ab*$^{\mathrm{v}}$	2.229 (9)	S1*cd*—O2*cd*	1.49 (1)
Cd1—O3*ef*	2.251 (9)	S1*cd*—O3*cd*	1.50 (1)
		S1*cd*—O4*cd*	1.475 (9)
O1*ab*—S1*ab*—O2*ab*	108.3 (6)	O2*cd*—S1*cd*—O3*cd*	110.6 (6)
O1*ab*—S1*ab*—O3*ab*	107.4 (6)	O2*cd*—S1*cd*—O4*cd*	110.3 (6)
O1*ab*—S1*ab*—O4*ab*	111.2 (6)	O3*cd*—S1*cd*—O4*cd*	109.1 (6)
O2*ab*—S1*ab*—O3*ab*	110.6 (6)	O1*ef*—S1*ef*—O2*ef*	108.3 (6)
O2*ab*—S1*ab*—O4*ab*	110.3 (6)	O1*ef*—S1*ef*—O3*ef*	107.4 (6)
O3*ab*—S1*ab*—O4*ab*	109.1 (6)	O1*ef*—S1*ef*—O4*ef*	111.2 (6)
O1*cd*—S1*cd*—O2*cd*	108.3 (6)	O2*ef*—S1*ef*—O3*ef*	110.6 (6)
O1*cd*—S1*cd*—O3*cd*	107.4 (6)	O2*ef*—S1*ef*—O4*ef*	110.3 (6)
O1*cd*—S1*cd*—O4*cd*	111.2 (6)	O3*ef*—S1*ef*—O4*ef*	109.1 (6)

Symmetry codes: (i) $\frac{1}{2}+x, \frac{3}{2}-y, 1-z$; (ii) $1-x, \frac{1}{2}+y, \frac{3}{2}-z$; (iii) $\frac{3}{2}-x, 1-y, \frac{1}{2}+z$; (iv) $-x, y-\frac{1}{2}, \frac{1}{2}-z$; (v) $\frac{1}{2}-x, 1-y, z-\frac{1}{2}$; (vi) $1-x, y-\frac{1}{2}, \frac{1}{2}-z$; (vii) $x-\frac{1}{2}, \frac{1}{2}-y, -z$; (viii) $\frac{1}{2}-x, -y, z-\frac{1}{2}$; (ix) $x-\frac{1}{2}, \frac{1}{2}-y, 1-z$.

Table 5
Chain-adapted symmetry modes compatible with the $P2_1$ symmetry for the atoms in the 4(*a*) Wyckoff positions of the $P2_13$ space group.

The four atoms follow the labelling scheme of the *International Tables for Crystallography* (1992, Vol. A).

	Chain adapted modes					
	$P2_13$	$P2_12_12_1$		$P2_1$		
Atomic labels	φ_1	φ_2	φ_3	φ_4	φ_5	φ_6
(1) x, x, x	111	$1\overline{\tfrac{1}{2}}\overline{\tfrac{1}{2}}$	$01\bar{1}$	100	010	001
(4) $-x+\frac{1}{2}, -x, x+\frac{1}{2}$	$\bar{1}\bar{1}1$	$\bar{1}\tfrac{1}{2}\overline{\tfrac{1}{2}}$	$0\bar{1}\bar{1}$	$\bar{1}00$	$0\bar{1}0$	001
(3) $-x, x+\frac{1}{2}, -x+\frac{1}{2}$	$\bar{1}1\bar{1}$	$\bar{1}\overline{\tfrac{1}{2}}\tfrac{1}{2}$	011	100	$0\bar{1}0$	001
(4) $x+\frac{1}{2}, -x+\frac{1}{2}, -x$	$1\bar{1}\bar{1}$	$1\tfrac{1}{2}\tfrac{1}{2}$	$0\bar{1}1$	$\bar{1}00$	010	001
N	$1/(12)^{1/2}$	$1/6^{1/2}$	$1/8^{1/2}$	1/2	1/2	1/2

the refinement. The scale factors for each group were then refined, keeping the remaining parameters fixed with respect to the first refined model ($R \simeq 16\%$).

The origin of these scale factors is obscure, but some hints can be obtained by plotting (see Fig. 3) the different groups of intensities (with their scale factor) *versus* the absorption correction A applied to the measured intensities

$$I_{\rm obs} = I_m/A,$$

where I_m and $I_{\rm obs}$ are the measured and observed intensities corrected for absorption, respectively.

From the histograms of Fig. 3 (corresponding to the monoclinic phase), it can be seen that for small values of scale factors, the intensities are located in the region corresponding to high values of A (short average X-ray path within the sample), and *vice versa*, for large values of scale factors the intensities are localized in the region of small A values. The additional scale factors palliate a deficient absorption correction owing to the screening among the domains, typical in a multidomains sample which is highly absorbent. Up to now, effective methods for the correct treatment of these problems were not known.

Once the scale factors (Sf_i) of the different reflection groups (F_i) were refined, a new reflection file was built applying to each group of reflections the corresponding scale factor using the following expression

$$I_o(\text{rescaled}) = (I_o)_i/(Sf_i)^2.$$

After having the new reflection file with rescaled intensities, we restarted the refinement procedure in the monoclinic phase. A few cycles later, some anisotropic displacement parameters for some Cd atoms become non-positive definite, therefore, they were refined isotropically in the remaining cycles. Final R (wR) converged to 0.044 (0.062). The final volume fractions of the six domains show that there are three predominant domains 1, 3 and 5 (Table 1). The symmetry operations relating the three orientation states are threefold axes and the sum of each one with the corresponding antiparallel (‘$+x_i$, $-x_i$’) axis represent approximately a third of the total volume of the crystal. The apparent presence of only three domains in the monoclinic phase is probably related at least in part to the small monoclinic lattice distortion and therefore to the perfect superposition of the reflections proceeding from antiparallel domains. The homogeneous distribution of the ferroelastic domains was also observed by optical observation of the domains.

In the orthorhombic phase (85 K) the reflection intensities were treated as for those of the monoclinic phase. Almost at the end of the refinement the anisotropic displacement parameters for some O atoms become non-positive definite. Therefore, all the U^{ij} components were kept fixed for the O and S atoms forming the SO_4 tetrahedra. This restriction does not affect the final results, especially the atomic positions. The final R (wR) values were 0.057 (0.060). The final volume fractions of orthorhombic domains are listed in Table 1, showing a predominant domain with 79.1% of the total volume of the

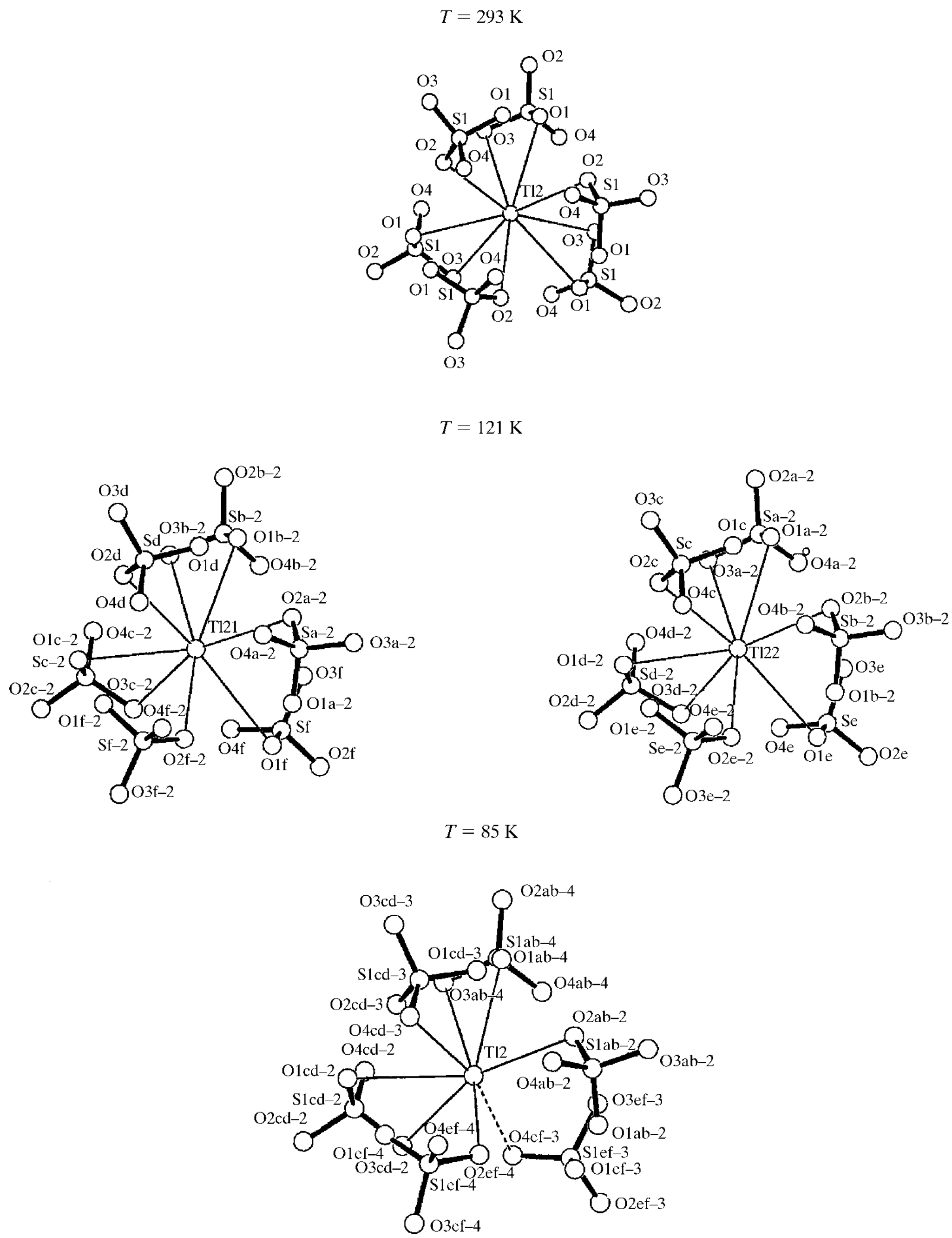

(*a*)

Figure 4
Reconstruction of (*a*) the Tl2—O and (*b*) the Tl1—O contacts in the monoclinic and orthorhombic phases. The dashed lines represent the new established contacts with respect to the cubic phase.

sample. This result is in good agreement with optical observation of the domains and with the fact that in the orthorhombic phase domain walls are not permissible (Sapriel, 1975).

In order to evaluate the correctness of the absolute structure, the inverted structures in both monoclinic and triclinic phases were also refined, leading to a (significantly) worse result (in terms of the R factor).

The atomic parameters of both monoclinic and orthorhombic phases are reported in Table 3. Selected bond distances and angles are given in Table 4.

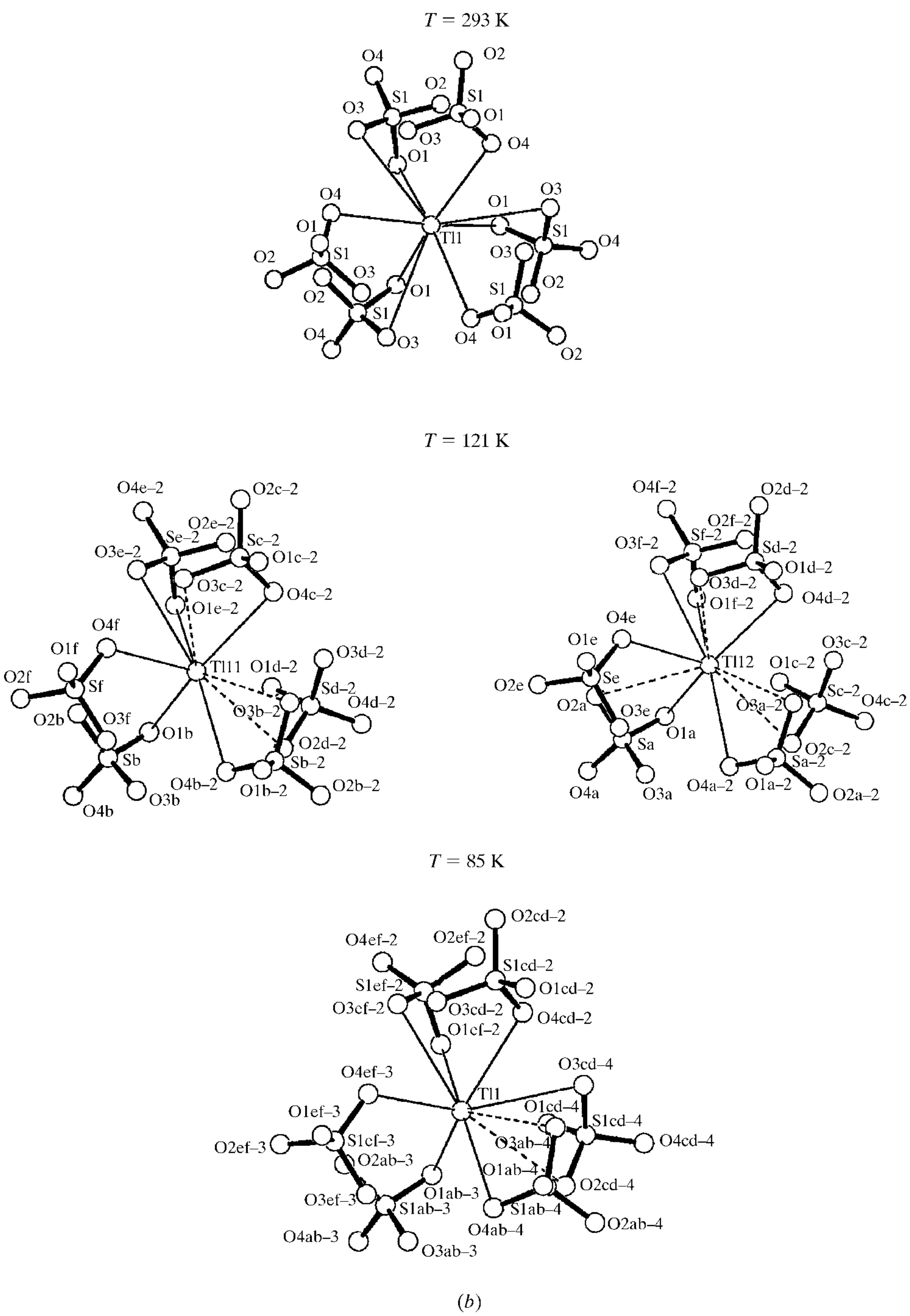

Figure 4 (continued)

3. Symmetry distortion analysis of the monoclinic phase

A quantitative comparison of the experimental structures of the monoclinic and cubic phases is sufficient for determining the total structural distortion that relates them, but the separation of the unstable primary mode, which triggers the transition, from the secondary modes requires some symmetry analysis of the global distortion.

The global distortion can be formally described in terms of *chain-adapted* modes, where the atomic displacement is decomposed in displacements of different symmetry which appear in the group–subgroup chain relating the space groups of both the high- and low-temperature structures

$$u_\alpha(l,\kappa) = \sum_Z \sum_i C^Z(i)\xi^Z_\alpha(\kappa, l|i), \tag{1}$$

where the first sum in (1) is over all possible space groups Z, such that $G > Z > H$, including the trivial cases G and H. A decomposition of this type was first introduced by Rae *et al.* (1990).

The atomic displacement field $u_\alpha(l,\kappa)$ represents the displacement of each atom (l,κ) in the low-symmetry structure. κ is the atomic label within the corresponding unit cell l of the high-symmetry structure and α represents the three independent components (x, y, z). ξ and C are the polarization vector and the amplitudes of the symmetry mode, respectively. For each group Z, several modes in (1) can exist and the index i runs over them.

The symmetry chain-adapted modes were constructed using the method described by Aroyo & Pérez-Mato (1998) and the information given in the *International Tables of Crystallography* (1992, Vol. A). Table 5 shows the structure of the different symmetry-adapted modes for atoms at the Wyckoff position 4(a). There are the following modes: one $P2_13$ symmetry mode φ_1, two modes with symmetry $P2_12_12_1$ (φ_2 and φ_3) and three $P112_1$ symmetry-adapted modes (φ_4, φ_5 and φ_6). For atoms at the Wyckoff position 12(b)

Table 6
Chain-adapted symmetry modes compatible with the $P2_1$ symmetry for the atoms in the 12(b) Wyckoff positions of the $P2_13$ space group.

The 12 atoms follow the labelling scheme of the *International Tables for Crystallography* (1992, Vol. A).

	$P2_13$ modes			$P2_12_12_1$ modes						$P2_1$ modes								
Atomic labels	ϕ_1	ϕ_2	ϕ_3	ϕ_4	ϕ_5	ϕ_6	ϕ_7	ϕ_8	ϕ_9	ϕ_{10}	ϕ_{11}	ϕ_{12}	ϕ_{13}	ϕ_{14}	ϕ_{15}	ϕ_{16}	ϕ_{17}	ϕ_{18}
(1) x, y, z	100	010	001	100	010	001	000	000	000	100	010	001	000	000	000	000	000	000
(2) $-x+\frac{1}{2}, -y, z+\frac{1}{2}$	$\bar{1}00$	$0\bar{1}0$	001	$\bar{1}00$	$0\bar{1}0$	001	000	000	000	$\bar{1}00$	$0\bar{1}0$	001	000	000	000	000	000	000
(3) $-x, y+\frac{1}{2}, -z+\frac{1}{2}$	$\bar{1}00$	010	$00\bar{1}$	$\bar{1}00$	010	$00\bar{1}$	000	000	000	100	$0\bar{1}0$	001	000	000	000	000	000	000
(4) $x+\frac{1}{2}, -y+\frac{1}{2}, -z$	100	$0\bar{1}0$	$00\bar{1}$	100	$0\bar{1}0$	$00\bar{1}$	000	000	000	$\bar{1}00$	010	001	000	000	000	000	000	000
(5) z, x, y	010	001	100	$0\bar{\tfrac{1}{2}}0$	$00\bar{\tfrac{1}{2}}$	$\bar{\tfrac{1}{2}}00$	010	001	100	000	000	000	100	010	001	000	000	000
(6) $z+\frac{1}{2}, -x+\frac{1}{2}, -y$	$0\bar{1}0$	$00\bar{1}$	100	$0\tfrac{1}{2}0$	$00\tfrac{1}{2}$	$\bar{\tfrac{1}{2}}00$	$0\bar{1}0$	$00\bar{1}$	100	000	000	000	$\bar{1}00$	010	001	000	000	000
(7) $-z+\frac{1}{2}, -x, y+\frac{1}{2}$	$0\bar{1}0$	001	$\bar{1}00$	$0\tfrac{1}{2}0$	$00\bar{\tfrac{1}{2}}$	$\tfrac{1}{2}00$	$0\bar{1}0$	001	$\bar{1}00$	000	000	000	$\bar{1}00$	$0\bar{1}0$	001	000	000	000
(8) $-z, x+\frac{1}{2}, -y+\frac{1}{2}$	010	$00\bar{1}$	$\bar{1}00$	$0\bar{\tfrac{1}{2}}0$	$00\tfrac{1}{2}$	$\tfrac{1}{2}00$	010	$00\bar{1}$	$\bar{1}00$	000	000	000	100	$0\bar{1}0$	001	000	000	000
(9) y, z, x	001	100	010	$00\bar{\tfrac{1}{2}}$	$\bar{\tfrac{1}{2}}00$	$0\bar{\tfrac{1}{2}}0$	$00\bar{1}$	$\bar{1}00$	$0\bar{1}0$	000	000	000	000	000	000	100	010	001
(10) $-y, z+\frac{1}{2}, -x+\frac{1}{2}$	$00\bar{1}$	$\bar{1}00$	010	$00\tfrac{1}{2}$	$\tfrac{2}{2}00$	$0\bar{\tfrac{1}{2}}0$	001	100	$0\bar{1}0$	000	000	000	000	000	000	100	$0\bar{1}0$	001
(11) $y+\frac{1}{2}, -z+\frac{1}{2}, -x$	$00\bar{1}$	100	$0\bar{1}0$	$00\tfrac{1}{2}$	$\bar{\tfrac{1}{2}}00$	$0\tfrac{1}{2}0$	001	$\bar{1}00$	010	000	000	000	000	000	000	$\bar{1}00$	010	001
(12) $-y+\frac{1}{2}, -z, x+\frac{1}{2}$	001	$\bar{1}00$	$0\bar{1}0$	$00\bar{\tfrac{1}{2}}$	$\tfrac{1}{2}00$	$0\tfrac{1}{2}0$	$00\bar{1}$	100	010	000	000	000	000	000	000	$\bar{1}00$	$0\bar{1}0$	001
N	$1/(12)^{1/2}$	$1/(12)^{1/2}$	$1/(12)^{1/2}$	$1/6^{1/2}$	$1/6^{1/2}$	$1/6^{1/2}$	$1/8^{1/2}$	$1/8^{1/2}$	$1/8^{1/2}$	1/2	1/2	1/2	1/2	1/2	1/2	1/2	1/2	1/2

Table 7
Amplitudes ($\times 10^5$) of the symmetry modes describing the monoclinic phase of $Tl_2Cd_2(SO_4)_3$, compared with the cubic structure at room temperature for atoms in the Wyckoff positions 4(a) of space group $P2_13$.

The amplitudes are given in relative units and are directly related to the atomic displacements. The values given in parentheses are the amplitudes obtained after fixing the origin forcing the z-coordinate of Tl21 to be the same in both the parent and monoclinic phases.

	Tl1	Tl2	Cd1	Cd2
φ_1	21.9	53.7	−8	−3.7
φ_2	30.6	19.6	486.6	73
φ_3	−36.7	19.4	182.4	41.7
φ_4	−63.5	−18.5	152.5	−174.5
φ_5	−20.5	43.5	44	40.5
φ_6	−792.5 (7.5)	−828 (−28)	−720 (80)	−945 (−145)

(Table 6) there are three $P2_13$ (ϕ_1, ϕ_2, ϕ_3), six $P2_12_12_1$ ($\phi_4,..., \phi_9$) and nine $P112_1$ symmetry-adapted modes ($\phi_{10},..., \phi_{18}$).

On the other hand, the symmetry modes as given in Tables 5 and 6 satisfy the orthogonality condition

$$\sum_{\kappa,\alpha} \xi_\alpha^{Z*}(\kappa|i)\xi_\alpha^Z(\kappa|i') = \|\xi_\alpha^Z(\kappa|i')\|^2\delta_{ii'}, \qquad (2)$$

where $\|\xi_\alpha^Z(\kappa|i)\|$ is the norm of a given mode and * represents complex conjugates. Once the symmetry-adapted modes $\xi_\alpha^Z(\kappa|i)$ and the displacement field $u_\alpha(l,\kappa)$ have been calculated, the amplitude of each mode can be determined by

$$C^Z(i) = (1/\|\xi_\alpha^Z(\kappa|i)\|^2)\sum_{\kappa,\alpha}\xi_\alpha^{Z*}(\kappa|i)u_\alpha(l,\kappa). \qquad (3)$$

The norm $\|\xi_\alpha^Z(\kappa|i)\|$ given to the modes in Tables 5 and 6 has not been chosen as unity to relate directly the magnitudes of the amplitudes $C^Z(i)$ to the atomic displacement. The displacement field $u_\alpha(l,\kappa)$ has been determined from the comparison of the ferroelectric phase and the high-temperature cubic phase, as described by Guelylah, Madariaga & Breczewski (1996). Owing to the polar character of the $P2_1$ space group the origin was fixed arbitrarily along the monoclinic z axis. In order to avoid a false high amplitude along the polar direction, during the comparison of the two structures the origin of the monoclinic phase was chosen to be the same as that of the cubic structure. The slight deformation of the Bravais lattice between the two phases can be avoided. The value of the amplitudes $C^Z(i)$ as obtained from (3) are shown in Tables 7 and 8 for atoms in special and general positions, respectively. The phase transition sequence in TCdS is very complicated, especially the III ↔ IV change, since the symmetry (orthorhombic) of the low-temperature phase IV is higher than those of the intermediate phases II and III. For that reason, the transition III ↔ IV cannot be considered of Landau type and a symmetry analysis cannot be applied to the distortion relating the structures of phases IV (orthorhombic) and III (triclinic). Nevertheless, the distortion relating the orthorhombic and the cubic phases can be decomposed in terms of symmetry modes of the latter one.

4. Results and discussion

The structure of the high-temperature phase of TCdS was previously refined using X-ray diffraction measurements (Guelylah, Madariaga & Breczewski, 1996). In the monoclinic structure the heavy atoms (Tl and Cd) are slightly displaced from their cubic positions. Larger displacements occur for atoms constituting the tetrahedral SO_4 groups, especially for O atoms. The displacement of SO_4 groups can be described by three translations and three rotations around the crystallographic axes. SO_4 groups present on average a regular form with the S—O distance varying from 1.452 (4) to 1.501 (4) Å and a mean value of 1.476 (4) Å. The O—S—O angles vary from 106.6 (3) to 113.5 (3)° with a mean value of 109.4 (3)°. The same behaviour of the SO_4 groups was observed in the

Table 8
Amplitudes ($\times 10^5$) of the symmetry modes describing the monoclinic phase of $Tl_2Cd_2(SO_4)_3$, compared with the cubic structure at room temperature for atoms in the Wyckoff positions 12(b) of space group $P2_13$.

The amplitudes are given in relative units and are directly related to the atomic displacements. The values given in parentheses are the amplitudes obtained after fixing the origin forcing the z coordinate of Tl21 to be the same in both the parent and monoclinic phases.

	S1	O1	O2	O3	O4
ϕ_1	−62.3	667.7	278.8	−434.1	−234.9
ϕ_2	31.7	736.98	−157.9	−351.9	−957.8
ϕ_3	−72.7	749.6	−715	−528.8	481.7
ϕ_4	423.3	291.8	514.8	232.2	634
ϕ_5	−558.4	−954.4	−663.8	−1228.4	555.6
ϕ_6	−103.9	−775.6	−771.1	767.5	333
ϕ_7	−458.9	−741.7	−567.8	−2209.3	1537.9
ϕ_8	33.5	26.8	−558.9	−556.5	1155
ϕ_9	−33.6	557.9	−2467.4	1171.3	725.5
ϕ_{10}	−164	−171	−166	−101.5	−214
ϕ_{11}	280	144.5	257	117.5	583
ϕ_{12}	−787 (15)	−1036 (−238)	−835.5 (−35.5)	−527 (273)	−742 (58)
ϕ_{13}	103.5	−317.5	321	256.5	147
ϕ_{14}	49	265	202.5	68	−329
ϕ_{15}	−754.5 (45)	−712.5 (87.5)	−1008 (−208)	−810.5 (−10.5)	−447.5 (352.5)
ϕ_{16}	−21.5	−160.5	143	−98.5	22
ϕ_{17}	17.5	123.5	−323	112	169.5
ϕ_{18}	−784 (15)	−1015.5 (−215)	−833.5 (−33.5)	−873 (−73)	−432.5 (377.5)

orthorhombic phase (85 K) with a smaller deformation in the (O—S—O) angles, varying from 107.40 (6) to 111.2 (6)°.

The nearest neighbours, O atoms, surrounding the Cd atoms form distorted octahedra. Oxygen–cadmium contacts are neither broken nor established at the phase transition. The distortion of the octahedra is due to the loss of the threefold axes where Cd atoms are located in the cubic phase. In the cubic phase, O atoms are generated by the application of the threefold axes giving rise to equilateral triangles, nevertheless, in the monoclinic phase all the O atoms are independent, therefore, the triangles are not equilateral. In all these octahedra of the monoclinic phase, the majority of Cd—O distances are shorter than in the cubic phase, being several O atoms closer to the Cd^{2+} cations. Owing to this movement, some O atoms are pushed out with Cd—O distances longer than in the high-temperature phase. In general, the average ⟨Cd—O⟩ distances appear to decrease in the monoclinic phase. In the orthorhombic phase the octahedra are less distorted and the average ⟨Cd—O⟩ distances are almost the same as in the monoclinic phase (Table 4). For langbeinites of type II (KCdS, KMnS and KCaS; Abrahams *et al.*, 1978; Percival *et al.*, 1989; Yamada *et al.*, 1981; Speer & Salje, 1986), the average distances ⟨B^{2+}—O⟩ (B = Cd, Mn, Ca) in the low-temperature orthorhombic phase are larger than in the cubic one. A precise analysis of the Cd position indicates that these atoms are out of the geometrical centres of the octahedra. The displacement is ~0.17 and 0.15 Å for Cd11 and Cd12, respectively, and 0.10 Å for Cd21 and Cd22. In the orthorhombic phase (85 K), the displacement is ~0.20 and 0.18 Å for Cd1 and Cd2, respectively.

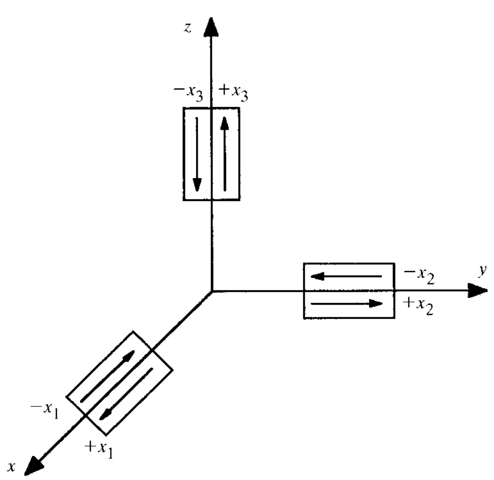

Figure 5
Scheme of the distribution of domains in the monoclinic phase of $Tl_2Cd_2(SO_4)_3$. The arrows indicate the polarization vector direction in the six orientational states.

The O atoms surrounding the monovalent (Tl) cations form more complicated and deformed polyhedra than in the cubic phase. Small Tl displacements together with SO_4 rotations are sufficient to change the number of Tl—O contacts. Around the independent Tl21 and Tl22 cations, it seems that the SO_4 groups exert the same rotation movement breaking one cubic contact Tl21—O3f and Tl22—O3e^{i} (Fig. 4a)[4] and they do not make any new contact remaining with a coordination of 8 within a sphere of 3.3 Å. For the Tl11 and Tl12 cations (Fig. 4b) the mechanism of contact reconstruction is very complicated. For both cations three of the cubic Tl—O contacts are broken in the monoclinic phase, two of them with the same tetrahedron (S1d and S1c^{i} for Tl11 and Tl12, respectively) and the last one with a different tetrahedron (S1b^{i} and S1a^{i} for Tl11 and T12, respectively). This loss of contacts is compensated by new ones. Tl11 establishes three new contacts with O atoms belonging to three different tetrahedra, retaining its coordination number as in the cubic phase (9). Nevertheless, Tl12 establishes four new contacts with four different tetrahedra, thus increasing its coordination number from 9 to 10. Even though the coordination about the Tl11 and Tl12 atoms is different, the movement of the (SO_4) groups surrounding each of them is almost the same. In the orthorhombic phase the coordination is 9 and 8 for Tl1 and Tl2, respectively. After this contact reconstruction in the low-temperature phases, the distances Tl11—O and Tl12—O at 121 K and Tl1—O at 85 K are shorter than in the cubic phase. For this reason the bond-valence sums (Brown & Altermatt, 1985; Brese & O'Keeffe, 1991) corresponding to the Tl11 and Tl12 polyhedra in the

[4] Symmetry code: (i) $-x, -y, \frac{1}{2}+z$.

Table 9
Bond-valence sums (v.u.) for atoms in the cubic, monoclinic (121 K) and orthorhombic (85 K) structures of $Tl_2Cd_2(SO_4)_3$.

For the sake of simplicity, in the monoclinic and orthorhombic structures the values given to the O atoms have been averaged among those atoms that are symmetry equivalent in the cubic phase.

	Cubic phase (298 K) (Guelylah, Madariaga & Breczewski, 1996)	Monoclinic phase (121 K)	Orthorhombic phase (85 K)
Tl1	0.61	0.87 (Tl11) 0.90 (Tl12)	0.94
Tl2	0.83	0.77 (Tl21) 0.81 (Tl22)	0.88
Cd1	2.13	2.35 (Cd11) 2.41 (Cd12)	2.24
Cd2	2.03	2.11 (Cd21) 2.24 (Cd22)	2.14
S	6.7	5.98	5.97
O1	1.96	2.09	2.12
O2	2.18	2.06	1.99
O3	2.17	1.91	1.92
O4	2.25	1.99	2.02

monoclinic phase and to the Tl1 polyhedron in the orthorhombic structure are closer to their chemical valence value, since in the cubic phase Tl1 atoms are loosely bonded (Guelylah, Madariaga & Breczewski, 1996). The values of the bond-valence sums calculated for the atoms forming the monoclinic and the orthorhombic structures are given in Table 9. The corresponding values in the cubic structure are also given for comparison. The coordination of Tl atoms in the monoclinic and orthorhombic phases can be compared with that of the known low-temperature orthorhombic phases of KCdS, KMnS and KCaS type II langbeinites (Abrahams *et al.*, 1978; Yamada *et al.*, 1981; Speer & Salje, 1986). In these compounds the coordination around the monovalent atoms is 10 and 9 for K1 and K2, respectively, which are different from those of Tl atoms occupying similar positions in the low-temperature phases of TCdS. Nevertheless, one could expect that the coordination in the orthorhombic phase can be the same as for type II compounds, which is not the case due to the differences in the amplitude and direction of SO_4 rotations.

As for langbeinite type II compounds, in the low-temperature phases of TCdS the SO_4 tetrahedra are rotated with respect to their cubic positions. Nevertheless, the angle and sense of rotation of SO_4 groups in the monoclinic and orthorhombic phases of TCdS are different from those observed in the orthorhombic phases of KCdS, KMnS and KCaS (Abrahams *et al.*, 1978; Yamada *et al.*, 1981; Speer & Salje, 1986; Guelylah, Aroyo & Perez-Mato, 1996). There the angle and the sense of rotations for each SO_4 are practically the same. In the monoclinic phase of TCdS (121 K) two independent tetrahedra belonging to the same orthorhombic orbit[5] rotate under almost orthorhombic symmetry, the rotated angles being practically identical (see Table 10). This is why the environment of the two independent Tl atoms are practically equivalent (see, for instance, Fig. 4, Tl11 with Tl12 and Tl21 with Tl22). The angle of rotation appears to increase as temperature decreases. Therefore, the rotations of the SO_4 tetrahedra in the orthorhombic phase are more important than those of the monoclinic structure. The sense of the orthorhombic rotations seems to be continuous with that observed in the monoclinic phase [see, for instance, in Table 10, $Rx(SO_4)ab$, $Ry(SO_4)cd$, $Rx(SO_4)ef$, respectively]. Nevertheless, between both phases another phase exists whose symmetry is triclinic (Brezina & Glogarova, 1972; Ikeda & Yasuda, 1975). Therefore, each monoclinic SO_4 tetrahedron will split into two independent ones. In the transition to the orthorhombic phase (III $\leftrightarrow$ IV), four independent triclinic tetrahedra must match their rotations to form an orthorhombic orbit. Therefore, the magnitude and sense of rotations in the triclinic phase must transform under 'pseudo-orthorhombic' symmetry, as observed in the monoclinic phase.

Ferroelectricity is symmetry-allowed in the monoclinic phase. The spontaneous polarization P_s along the polar axis has been measured by the pyroelectric current method (Ikeda & Yasuda, 1975). The value extracted from the experimental curve at 122 K is approximately equal to 0.07×10^{-2} Cm^{-2}. Using the method described by Abrahams & Keve (1971), we have calculated the dipole moments along the z direction from the structure obtained at 121 K using ionics species Tl^+, Cd^{2+}, S^{6+}, O^{2-} and the value obtained is 0.2×10^{-2} Cm^{-2}. The same value was obtained considering a point charge centred in the mass centre of the $(SO_4)^{2-}$ tetrahedra. The low experimental value of P_s obtained by dielectric measurements can be the consequence of the domain structure. For example, supposing a sample with a homogeneous distribution of domain structures in the monoclinic phase, the only domain contributing to the P_s measurement are those whose polar axis is oriented along the measurement direction, representing in this case the

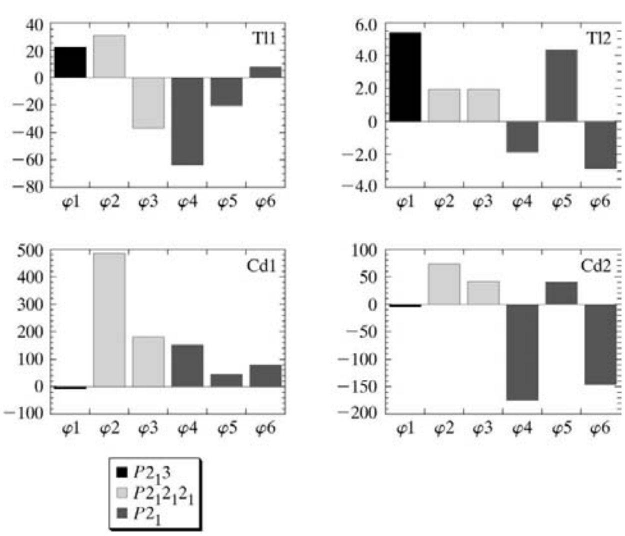

Figure 6
Amplitudes ($\times 10^5$) of the chain-adapted symmetry modes for atoms in the Wyckoff position 4(a) of the space group $P2_13$. The amplitudes are directly related to the atomic displacement.

[5] Group of atoms belonging to the same Wyckoff positions or a group of symmetry-equivalent atoms.

third part of the total volume of the crystal (see, for example, Fig. 5). Under this hypothesis the calculated value of P_s agrees very well with the experimental results of Ikeda & Yasuda (1975).

Fig. 6 represents the amplitudes of the modes for atoms in special positions, where it can be seen that in the ferroelectric distortion not only the primary $P2_1$ modes predominate, but also the $P2_13$ and $P2_12_12_1$ modes have comparable amplitudes. For some atoms such as Tl1 and Cd2, the amplitudes of the primary φ_4 mode is especially important, which represents a displacement along the x direction. The secondary distortions φ_1 and φ_2 for Tl2 and Cd1, respectively, have special weight in the global distortion of these atoms. Furthermore, for atoms occupying general positions (S and O), the contribution of the $P2_1$ primary modes to the total distortion is less important than those of the secondary ones (Fig. 7). For a displacive phase transition, one can expect that the global distortion can be described by the displacement of the primary modes, while the relative weight of the secondary modes is extremely weak (Mañes *et al.*, 1982; Zúñiga *et al.*, 1982; Gómez-Cuevas *et al.*, 1984; Pérez-Mato *et al.*, 1986). Nevertheless, for the $P2_13 \leftrightarrow P2_1$ phase transition in TCdS and especially for atoms in general positions (SO_4), the contribution of the primary modes is very weak compared with that of the secondary ones. In the monoclinic structure of TCdS (121 K), the deformations which appear in the CdO_6 octahedra and the reconstruction of the Tl—O contacts are directly related to the (SO_4) rotations. Also, the environment around the two independent monovalent (Tl) and the two independent divalent (Cd) atoms (equivalent in the cubic and orthorhombic phases) is similar. This similarity in the envir-

Table 10
Rotations (°) of the symmetry-independent SO_4 tetrahedra in the monoclinic (121 K) and orthorhombic (85 K) structures with respect to the cubic structure.

The symmetry operations relating the coordinates of the different tetrahedra with the coordinates (x, y, z) of the only independent tetrahedron in the cubic phase are listed below.

	T = 121 K				T = 85 K		
	Rx	Ry	Rz		Rx	Ry	Rz
$(SO_4)a$	−3.70	2.26	−2.15	$(SO_4)ab$	−10.97	−5.72	1.39
$(SO_4)b$	−1.80	−2.75	2.38				
$(SO_4)c$	−5.51	−1.04	8.50	$(SO_4)cd$	−3.06	11.32	11.40
$(SO_4)d$	−3.71	−1.2	−11.40				
$(SO_4)e$	−6.81	1.10	9.29	$(SO_4)ef$	−23.05	0.12	8.74
$(SO_4)f$	−9.57	0.19	−10.09				

$(SO_4)a$ $x-\frac{1}{4}$; $(SO_4)ab$ x, y, z; $(SO_4)b$ $\frac{1}{2}+x-\frac{1}{4}, \frac{1}{2}-y, -z$; $(SO_4)c$ z, x, y $(SO_4)cd$ z, x, y; $(SO_4)d$ $\frac{1}{2}+z-\frac{1}{4}, \frac{1}{2}-x, -y$; $(SO_4)e$ y, z, x $(SO_4)ef$ y, z, x; $(SO_4)f$ $\frac{1}{2}+y-\frac{1}{4}, \frac{1}{2}-z, -x$.

onment of the polyhedra is due to the quasi-orthorhombic rotation of the SO_4 groups in the monoclinic phase and to the small displacement of the Cd and Tl atoms. These distortions are reflected in the amplitudes of the symmetry-adapted modes (Fig. 7). A Raman spectroscopy measurement (Rabkin *et al.*, 1979) showed that the distortion which appears in the monoclinic and triclinic phases is very weak, which agrees with the results of the present work. The authors also observed that there is some softening of the E-mode (Rabkin *et al.*, 1979) with frequency 17 cm^{-1} in the first phase transition. Curiously, the softening of this E-mode must be due to the $P2_13 \leftrightarrow P2_12_12_1$ phase transition. Therefore, it is not clear why we have first a phase transition to $P2_1$ and $P1$ phases, and finally to $P2_12_12_1$ and this is why the amplitudes of the monoclinic symmetry-adapted modes are very weak compared with those of orthorhombic ($P2_12_12_1$) symmetry, showing the monoclinic

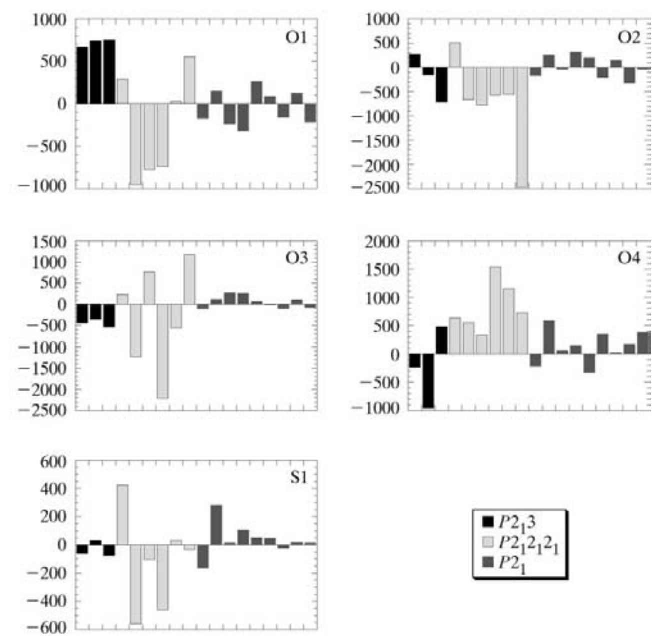

Figure 7
Amplitudes (× 10^5) of the chain-adapted symmetry modes for atoms in the Wyckoff position 12(b) of the space group $P2_13$. The amplitudes are directly related to the atomic displacement.

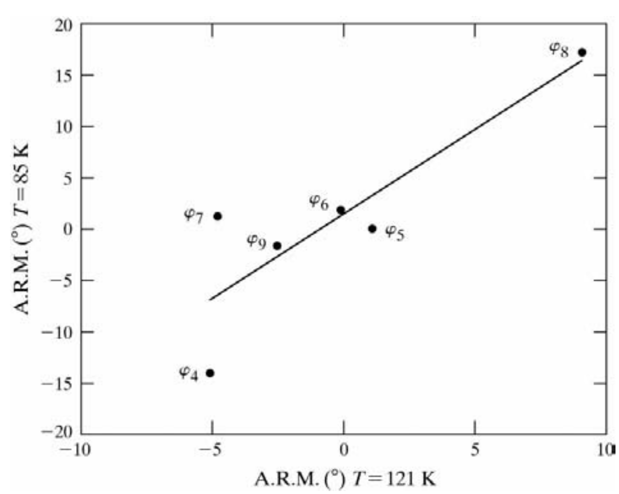

Figure 8
Representation of the amplitudes of the rotational $P2_12_12_1$ symmetry modes obtained from the symmetry mode analysis of the orthorhombic structure (85 K) against the corresponding ones in the monoclinic structure (121 K).

structure to have a strong orthorhombic pseudosymmetry. From these results, one can suggest that the first phase transition in TCdS is to the orthorhombic phase with a slight additional monoclinic distortion. In the second phase transition the small amount of monoclinic distortion is split into a triclinic one and then finally in the transition to the orthorhombic phase all these additional distortions disappear, giving rise to a stable phase.

To stress the pseudo-orthorhombic character of the monoclinic distortion, the rotations of the tetrahedra in the monoclinic and orthorhombic phases can again be described by means of symmetry modes of the cubic one in a form analogous to equation (1). In Fig. 8, the amplitudes of the $P2_12_12_1$ modes at 121 K are compared with corresponding ones at 85 K. The points have been fitted to a straight line with slope 1.65. The large deviation of the ϕ_4 and ϕ_7 modes are due to the abrupt jump of the rotations Rx and Ry in the orthorhombic phase (see Table 10) corresponding to the tetrahedra $(SO_4)ab$ and $(SO_4)cd$, respectively. Nevertheless, the result shows that the $P2_12_12_1$ modes (primary in the orthorhombic phase and secondary in the monoclinic one) maintain essentially the same structure in both phases, changing only their global amplitudes by a factor of 1.65.

5. Conclusions

Up to now, type II langbeinite were the only compounds of the family whose structures at high and low temperature are known. The resolution of those structures was of great interest for the understanding of the phase transition mechanism in those compounds. However, for type I langbeinite, owing to the lack of structural information corresponding to the low-temperature phases, the mechanisms responsible for the phase transition and the factors behind the different phase transition schemes were still obscure. In the same way some results obtained by different experiments were not interpretable.

The resolution of the monoclinic and orthorhombic structures of TCdS reveal some factors responsible for the phase transition. Together with a small displacement of the heavy atoms, the rotations of SO_4 groups seem to be the most important effect after the phase transitions and differs in both types of langbeinites. The sense of rotation of these tetrahedra observed in the monoclinic and the orthorhombic phases of TCdS is opposite to that observed in the orthorhombic phases of type II compounds. Also, the rotation amplitudes are different, being smaller in TCdS. Despite these differences the most important structural change in both types of compounds seems to be the phase transition that relates the cubic $P2_13$ and orthorhombic $P2_12_12_1$ structures. In fact, the rotation of the sulfate tetrahedra in the orthorhombic phase of TCdS is continuous with that occurring in the monoclinic structure, in spite of the presence of a triclinic phase between them. Such a rotation, markedly pseudo-orthorhombic, accompanies smaller displacements of lower symmetry which force the intermediate phases in type I langbeinites.

This work has been supported by the Spanish Comisión Interministerial de Ciencia y Tecnología (project PB 94–1362).

References

Abrahams, S. C. & Keve, E. T. (1971). *Ferroelectrics*, **2**, 129–154.
Abrahams, S. C., Lissalde, F. & Bernstein, J. L. (1978). *J. Chem. Phys.* **68**, 1926–1935.
Aroyo, M. I. & Perez-Mato, J. M. (1998). *Acta Cryst.* A**54**, 19–30.
Artman, J. I. & Boerio-Goates, J. (1992). *Ferroelectrics*, **132** 141–152.
Brese, N. E. & O'Keeffe. (1991). *Acta Cryst.* B**47**, 192–197.
Brezina, B. & Glogarova, M. (1972). *Phys. Status Solidus A*, **11**, K39–42.
Brezina, B. & Havránková, M. (1974). *J. Cryst. Growth*, **21**, 77–81.
Brown, I. D. & Altermatt, D. (1985). *Acta Cryst.* B**41**, 244–247.
Cao, H., Dalley, N. K. & Boerio-Goates, J. (1993). *Ferroelectrics*, **146**, 45–56.
Cosier, J. & Glazer, A. M. (1986). *J. Appl. Cryst.* **19**, 105–107.
Dvorák, V. (1972). *Phys. Status Solidus B*, **52**, 93–98.
Eichhorn, K. (1987). *REDUCE.* DESY/HASYLAB, Unpublished.
Eichhorn, K. (1992). *AVSORTS*. DESY/HASYLAB, Unpublished.
Eichhorn, K. & Morgenroth, W. (1996). *DIF4 Kappa Diffractometer (HASYLAB Beamline F1) User Guide*. Karlsruhe, Hamburg, Germany.
Enraf–Nonius (1989). *CAD4 Software*, Version 5.0. Delft, The Netherlands.
Flack, H. D. (1974). *Acta Cryst.* A**30**, 569–573.
Franke, V., Hegenbarth, E. & Brezina, B. (1975). *Phys. Status Solidus A*, **28**, K77–80.
Glogarova, M. & Fousek, J. (1973). *Phys. Status Solidus A*, **13**, 579–590.
Glogarova, M., Fousek, J. & Brezina, B. (1972). *J. Phys.* **33**, C2, 75–76.
Gómez-Cuevas, A, Pérez-Mato, J. M., Tello, M. J., Madariaga, G., Fernandez, J., López Echarri, A., Zúñiga, F. J. & Chapuis, G. (1984). *Phys. Rev. B*, **29**, 2655–2663.
Guelylah, A., Aroyo, M. I. & Perez-Mato, J. M. (1996). *Phase Transit.* **59**, 155–179.
Guelylah, A., Madariaga, G. & Breczewski, T. (1996). *Acta Cryst.* C**52**, 2954–2956.
Hall, S. R., Flack, H. D. & Stewart, J. M. (1992). *Xtal3.2 Reference Manual*. Universities of Western Australia, Australia, Geneva, Switzerland, and Maryland, USA.
Hatch, D. M., Artman, J. I. & Boerio-Goates, J. (1990). *Phys. Chem. Miner.* **17**, 334–343.
Hikita, T., Chubachi, Y. & Ikeda,T. (1978). *J. Phys. Soc. Jpn*, **44**, 525–528.
Ikeda, T. & Yasuda, G. (1975). *Jpn. J. Appl. Phys.* **14**, 1287–1290.
Itoh, K., Ukeda, T. & Nakamura, E. (1992). *J. Phys. Soc. Jpn*, **61**, 4657–4658.
Kahrizi, M. & Steinitz, M. O. (1988). *Solid State Commun.* **66**, 375–378.
Kuroiwa, Y., Liu, M., Finlayson, T. R., Smith, T. F. & Itoh, K. (1997). *J. Phys. Soc. Jpn*, **66**, 1840–1841.
Lehmann, M. S. & Larsen, F. K. (1974). *Acta Cryst.* A**30**, 580–584.
Lissalde, F., Abrahams, S. C., Bernstein, J. L. & Nassau. K. (1979). *J. Appl. Phys.* **50**, 845–851.
Mañes, J. L., Tello, M. J. & Pérez-Mato, J. M. (1982). *Phys Rev. B*, pp. 250–268.
Moriyoshi, C. & Itoh, K. (1996). *J. Phys. Soc. Jpn*, **65**, 3537–3543.
Ng, H. N. & Calvo, C. (1975). *Can. J. Chem.* **53**, 1449–1455.
Percival, M. J. L., Schmahl, W. W. & Salje, E. (1989). *Phys. Chem. Miner.* **16**, 569–575.

Pérez-Mato, J. M., Gaztelua, F., Madariaga, G. & Tello, J. M. (1986). *J. Phys. C*, **19**, 1923–1935.
Petricek, V. & Dusek, M. (1998). *JANA*98 *Reference Manual.* Institute of Physics, Academy of Sciences of the Czech Republic.
Rabkin, L. M., Torgashov, V. I., Latush, L. T., Brezina, B. & Shuvalov, L. A. (1979). *Sov. Phys. Crystallogr.* **24**, 280–287.
Rae, D., Thompson, J. G., Withers, R. L. & Willis, A. (1990). *Acta Cryst.* B**46**, 474–487.
Sapriel, J. (1975). *Phys. Rev. B*, **12**, 5128–5140.
Speer, D. & Salje, E. (1986). *Phys. Chem. Miner.* **13**, 17–24.
Ukeda, T., Itoh, K. & Moriyoshi, C. (1995). *J. Phys. Soc. Jpn*, **64**, 504–512.
Yamada, N., Hikita, T., Maeda, M. & Ikeda, T. (1980). *J. Phys. Soc. Jpn*, **49** (Suppl. B), 102–107.
Yamada, N. & Kawano, S. (1977). *J. Phys. Soc. Jpn*, **43**, 1016–1020.
Yamada, N., Maeda, M. & Adachi, H. (1981). *J. Phys. Soc. Jpn*, **50**, 907–913.
Zemann, A. & Zemann, J. (1957). *Acta Cryst.* **10**, 409–413.
Zúñiga, F. J., Chapuis, G., Mañes, J. L. & Pérez-Mato, J. M. (1982). *J. Phys. C*, **15**, 5195–5201.